The EMBO Journal Vol. 21 No. 18 pp. 4841–4850, 2002

Nonself recognition is mediated by HET-C heterocomplex formation during vegetative incompatibility

Sovan Sarkar[1], Gopal Iyer[1], Jennifer Wu[2,3] and N.Louise Glass[1,4]

[1]Plant and Microbial Biology Department, 111 Koshland Hall, University of California, Berkeley, CA 94720, USA and
[2]The Biotechnology Laboratory and the Botany Department, University of British Columbia, Vancouver, British Columbia V6T 1Z3, Canada

[3]Present address: Clinical Research Division, Fred Hutchinson Cancer Research Center, Seattle, WA 98109, USA

[4]Corresponding author
e-mail: Lglass@uclink.berkeley.edu

S.Sarkar and G.Iyer contributed equally to this work

Nonself recognition during vegetative growth in filamentous fungi is mediated by heterokaryon incompatibility (*het*) loci. In *Neurospora crassa*, *het-c* is one of 11 *het* loci. Three allelic specificity groups, termed *het-c*^{OR}, *het-c*^{PA} and *het-c*^{GR}, exist in natural populations. Heterokaryons or partial diploids that contain *het-c* alleles of alternative specificity show severe growth inhibition, repression of conidiation and hyphal compartmentation and death (HCD). Using epitope-tagged HET-C, we show that nonself recognition is mediated by the presence of a heterocomplex composed of polypeptides encoded by *het-c* alleles of alternative specificity. The HET-C heterocomplex localized to the plasma membrane (PM); PM-bound HET-C heterocomplexes occurred in all three *het-c* incompatible allelic interactions. Strains containing *het-c* constructs deleted for a predicted signal peptide sequence formed HET-C heterocomplexes in the cytoplasm and showed a growth arrest phenotype. Our finding is a step towards understanding nonself recognition mechanisms that operate during vegetative growth in filamentous fungi, and provides a model for investigating relationships between recognition mechanisms and cell death.

Keywords: *Neurospora crassa*/nonself recognition/protein targeting/vegetative incompatibility

Introduction

Protein–protein interactions that mediate recognition of self and nonself have a fundamental role in many biological processes. Two distinct molecular mechanisms operate in self/nonself recognition. One mechanism operates via the recruitment of receptor ligands to accomplish allele-specific recognition. In flowering plants, gametophytic self-incompatibility is mediated by a receptor kinase encoded by the *S* locus (Nasrallah, 2000). At the mammalian major histocompatibility complex (MHC) loci, self and nonself MHC class I molecules are discriminated via MHC-antigen ligand and T-cell surface receptor (Jones *et al*., 1998). A second method for self/nonself discrimination involves combinatorial interactions of proteins to generate heterocomplexes with new regulatory functions. In fungi, combinatorial interactions between homeodomain proteins that function as transcriptional modulators have been described in several mating-type systems, such as the Mat **a1**p and Mat **α2**p in *Saccharomyces cerevisiae* (Ho *et al*., 1994), *b* locus gene-pair products in *Ustilago maydis* (Kämper *et al*., 1995) and the HD1 and HD2 polypeptides in *Coprinus cinereus* (Asante-Owusu *et al*., 1996).

In ascomycete fungi, nonself recognition during vegetative growth is mediated by vegetative (or heterokaryon) incompatibility. Different isolates are capable of undergoing hyphal fusion to form a heterokaryon, in which genetically different nuclei co-exist in a common cytoplasm. There are postulated benefits to heterokaryon formation, such as functional diploidy and mitotic recombination (Pontecorvo, 1956). The ability to form stable heterokaryons is regulated by heterokaryon (*het*) incompatibility loci (Glass *et al*., 2000; Saupe, 2000). Hyphal fusion between strains that differ in allelic specificity at a *het* locus generally results in rapid septal plugging and death of the fusion cell, a process referred to as hyphal compartmentation and death (HCD) (Garnjobst and Wilson, 1956; Jacobson *et al*., 1998; Wu and Glass, 2001). Nonself recognition mediated by *het* loci is thought to provide a protective mechanism to prevent transmission of infectious cytoplasmic elements, such as mycoviruses and senescence plasmids, and from exploitation by 'aggressive' genotypes (Debets and Griffiths, 1998; Cortesi *et al*., 2001).

In *Neurospora crassa*, 11 *het* loci have been genetically identified that regulate nonself recognition during vegetative growth (Perkins *et al*., 2000). At the *het-c* locus, isolates from natural populations fall into one of three *het-c* allelic specificity groups (Howlett *et al*., 1993; Saupe and Glass, 1997). These three allelic specificities are referred to as *het-c*^{OR}, *het-c*^{PA} and *het-c*^{GR} (Saupe *et al*., 1996; Saupe and Glass, 1997). Transformants, heterokaryons or partial diploids containing *het-c* alleles of alternative specificity show severe growth inhibition, are aconidial and show HCD (Perkins, 1975; Howlett *et al*., 1993; Saupe and Glass, 1997; Jacobson *et al*., 1998; Wu and Glass, 2001). Phylogenetic analysis of *het-c* among different species and genera of filamentous fungi related to *N.crassa* shows that polymorphisms associated with *het-c* allelic specificity are subject to balancing selection (Wu *et al*., 1998). Thus, *het-c* displays an evolutionary pattern similar to other self/nonself recognition loci, such as the MHC loci and the *S* locus in plants (Klein *et al*., 1998), and the *B* mating-type locus of *C.cinereus* (May *et al*., 1999).

The *het-c* locus encodes an ~960 amino acid protein (depending on the allele) with an N-terminal signal peptide

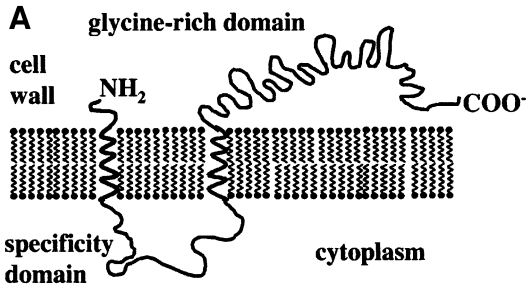

B

```
HET-C^OR FPHVGTDTRITLRNDTRNNG---------------KSVWPLVTGTFGG
HET-C^PA FPHVGTATKLKL-----ENRQFRRVRPGEGYDSGAKYAWPLVTGTFGG
HET-C^GR FPHVGTATQITL-----NNG---------------KLVWPLVTGTFGG
```

Fig. 1. Schematic diagram of HET-C. (**A**) HET-C is predicted to reside in the plasma membrane (http://psort.nibb.ac.jp/). (**B**) Amino acid sequence of the specificity domain of HET-C (Saupe and Glass, 1997). Allelic specificity (*het-c*^{OR}, *het-c*^{PA}, *het-c*^{GR}) is based on characterization of laboratory strains (Howlett *et al*., 1993; Saupe and Glass, 1997).

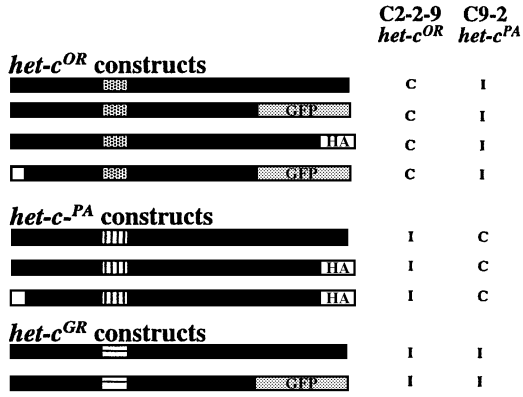

Fig. 2. Schematic diagram of epitope-tagged *het-c* constructs. N-terminal white boxes signify signal peptide deletion constructs. Patterned boxes indicate the *het-c* allelic specificity domain. GFP-tagged versions of *het-c*^{OR} and *het-c*^{GR} included the first 730 amino acids of HET-C^{OR} and 727 amino acids of HET-C^{GR}, which are fully functional forms (Saupe *et al*., 1996). The *het-c*^{PA} and *het-c*^{OR} HA-tagged constructs included DNA sequences for the nine amino acid HA-epitope tag fused to the 3′ end of the *het-c* open reading frame (ORF). Constructs were introduced into standard *het-c* tester strains C2-2-9 (*het-c*^{OR}) and C9-2 (*het-c*^{PA}) (Saupe and Glass, 1997) to test for function. C, compatible transformants; I, incompatible transformants. Differences in phenotype or *het-c* allelic specificity were not observed when tagged, untagged or *het-c* signal peptide deletion constructs were introduced into C2-2-9 or C9-2, when using either the *gpd* promoter or *het-c* promoter (see Materials and methods).

and a C-terminal glycine-rich domain, and is predicted to reside in the plasma membrane (Saupe *et al*., 1996) (Figure 1A). The structure and size of *het-c* polypeptides that confer alternative *het-c* specificity (HET-C^{OR}, HET-C^{PA} and HET-C^{GR}) are very similar, with the exception of a short region (30–48 amino acids) that differs in insertion/deletion (indel) pattern (Figure 1B). Allelic specificity at *het-c* is dependent upon this indel: swapping of this region between alleles switches *het-c* allelic specificity (Saupe and Glass, 1997; Wu and Glass, 2001).

In this study, we investigated the molecular mechanism of nonself recognition mediated by allelic differences at *het-c*. The simplest model describing *het-c* allelic recognition predicts either that heterocomplex formation between alternative *het-c* polypeptides is toxic to the cell or that its presence activates a pathway resulting in vegetative incompatibility. We show that nonself recognition is mediated by the physical interaction of HET-C polypeptides encoded by *het-c* alleles of alternative specificity. The HET-C heterocomplex specifically localizes to the plasma membrane of dead hyphal compartments. Deletion of a predicted signal peptide sequence in alternative *het-c* alleles led to cytoplasmic HET-C heterocomplex formation and a novel growth arrest phenotype. In all cases, co-expression of alternative *het-c* alleles resulted in stable HET-C heterocomplex formation.

Results

GFP- and HA-tagged versions of HET-C confer vegetative incompatibility

We used epitope-tagged *het-c* constructs in this study to assess HET-C localization and heterocomplex formation; alternative HET-C polypeptides (HET-C^{OR}, HET-C^{PA} and HET-C^{GR}) are 85–90% identical (Saupe and Glass, 1997). We used green fluorescent protein (GFP) (Cormack, 1998) and hemagglutinin (HA) (Forsburg and Sherman, 1997) as epitope tags (Figure 2). We confirmed the functionality of the epitope-tagged *het-c* constructs by introducing them into strains with different *het-c* allelic specificities (C9-2 *het-c*^{PA} and C2-2-9 *het-c*^{OR}) and via co-transformation into a *het-c* deletion strain, CJ44 (Wu and Glass, 2001). The phenotype displayed by transformants containing epitope-tagged *het-c* alleles (growth inhibition, repression of conidiation and ~20% HCD) was indistinguishable from a typical *het-c* incompatibility phenotype mediated by untagged *het-c* alleles (Figure 2).

HET-C localizes to the plasma membrane

HET-C is predicted to contain a signal peptide with a cleavage site at amino acids 29 and two transmembrane domains from amino acids 94–110 and 461–477. Thus, a mature, ~100 kDa HET-C protein is predicted to reside in the plasma membrane with the glycine-rich domain extending to the outside of the cell (Figure 1A).

Initially, we tried to localize HET-C::GFP in living hyphae of CJ44 (*het-c*^{OR}*::GFP*) compatible transformants by fluorescence microscopy. However, only high background fluorescence was detected (successful use of GFP for localization of fusion proteins in *Neurospora* has not been reported). We therefore chose the more sensitive analytical method of cell fractionation and western blot analysis to localize HET-C. The efficiency of our cell fractionation procedure was monitored using antibodies to the *N.crassa* plasma membrane H^+-ATPase (Figure 3C) (Bowman *et al*., 1981), and anti-β-tubulin antibodies (Figure 3D), a cytoplasmic fraction marker. The cell wall fraction is from the processed pellet following homogenization of mycelia and low speed centrifugation (1000 *g*). We introduced *het-c*^{OR}*::GFP* or *het-c*^{PA}*::HA* into CJ44, isolated hygromycin-resistant transformants and subjected them to cell fractionation, immunoprecipitation with anti-GFP or anti-HA antibodies, followed by western blot analysis. An expected HET-C^{OR}::GFP or

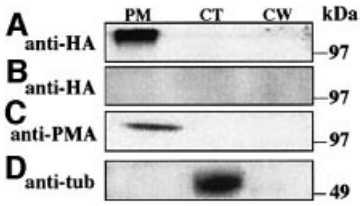

Fig. 3. HET-C is in the plasma membrane fraction. (**A**) CJ44 (*het-c^{PA}::HA*) compatible transformants were subjected to cell fractionation and anti-HA-aminolinked column chromatography. Eluates from cellular fractions were probed by western analysis with a monoclonal anti-HA antibody. (**B**) CJ44 (*het-c^{PA}*) compatible transformants treated identically to (A) show lack of cross-reacting material. (**C**) Western analysis using antibodies to the PM H^+-ATPase (Bowman *et al*., 1981) show the predicted ~100 kDa PM H^+-ATPase band. (**D**) Western analysis using antibodies to β-tubulin, a cytoplasmic marker. MW markers are indicated. PM, plasma membrane fraction; CT, cytoplasmic fraction; CW, cell wall fraction.

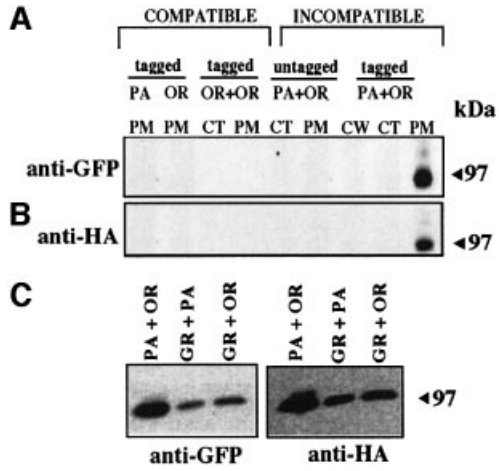

Fig. 4. HET-C^{PA}::HA and HET-C^{OR}::GFP form a heterocomplex in incompatible transformants. (**A**) Anti-HA antibody immunoprecipitated cellular fractions from CJ44 (*het-c^{OR}::GFP* + *het-c^{OR}::HA*) compatible and (*het-c^{OR}::GFP* + *het-c^{PA}::HA*) incompatible transformants and their untagged counterparts were subjected to western analysis using anti-GFP antibodies. (**B**) The blot in (A) was stripped in stripping buffer (62.5 mM Tris–HCl pH 7.6, 100 mM 2-mercaptoethanol, 5% SDS) at 55°C for 30 min, rinsed in PBS, blocked and re-probed with anti-HA antibody. HET-C homocomplexes were undetectable in CJ44 (*het-c^{OR}::GFP* + *het-c^{OR}::HA*) transformants (OR+OR tagged). PM, plasma membrane fraction; CT, cytoplasmic fraction; CW, cell wall fraction. (**C**) HET-C heterocomplex formation was detected in three *het-c* allelic combinations by co-immunoprecipitation experiments. Plasma membrane fractions were isolated from CJ44 (*het-c^{PA}::HA* + *het-c^{OR}::GFP*), (*het-c^{OR}::HA* + *het-c^{OR}::GFP*) and (*het-c^{OR}::HA* + *het-c^{GR}::GFP*) incompatible transformants and subjected to co-immunoprecipitation, as above. MW markers are indicated.

HET-C^{PA}::HA polypeptide of ~100 kDa was not detected in any of the cell fractions.

Because of our inability to detect HET-C by cell fractionation and immunoprecipitation, we resorted to the still more definitive approach of aminolink chromatography to enrich for HET-C in cellular fractions. We introduced *het-c^{PA}::HA* into CJ44, isolated transformants and subjected them to cell fractionation, as above. Each cellular fraction was passed through the anti-HA aminolinked column (see Materials and methods); bound proteins were eluted and subjected to western blot analysis using anti-HA antibodies. A protein with a molecular mass of ~100 kDa was detected from the plasma membrane fraction of CJ44 (*het-c^{PA}::HA*) transformants (Figure 3A). Cross-reacting proteins from untagged CJ44 (*het-c^{PA}*) transformants were not observed (Figure 3B). Thus, HET-C localized to the plasma membrane fraction, consistent with computational analyses.

Alternative HET-C polypeptides form a heterocomplex

The simplest model for *het-c*-mediated nonself recognition is that a HET-C heterocomplex is perceived by the hyphal compartment, which subsequently triggers vegetative incompatibility. We therefore assessed HET-C heterocomplex formation by cell fractionation and co-immunoprecipitation assays. We co-transformed tagged (*het-c^{OR}::GFP* + *het-c^{PA}::HA*) and untagged (*het-c^{OR}* + *het-c^{PA}*) alleles into CJ44, isolated incompatible transformants and subjected them to cell fractionation, immunoprecipitation using anti-HA antibodies, followed by western analysis using anti-GFP antibodies. In contrast to CJ44 (*het-c^{OR}::GFP*) or (*het-c^{PA}::HA*) compatible transformants, a protein of estimated molecular mass of ~100 kDa was detected in the plasma membrane fraction from CJ44 (*het-c^{OR}::GFP* + *het-c^{PA}::HA*) incompatible transformants by western analysis using anti-GFP antibodies (Figure 4A). The presence of HET-C^{PA}::HA in the fraction was confirmed by stripping the immunoblot and re-probing with anti-HA antibody (Figure 4B). Reciprocal co-immunoprecipitation assays gave an identical result (see Supplementary data available at *The EMBO Journal* Online); a HET-C heterocomplex was identified specifically in the plasma membrane fraction from epitope-tagged incompatible transformants.

We determined the ability of HET-C^{OR} to form a homocomplex by assessing cell fractions from CJ44 (*het-c^{OR}::GFP* + *het-c^{OR}::HA*) compatible transformants by co-immunoprecipitation assays. Unlike the HET-C^{OR}::GFP + HET-C^{PA}::HA heterocomplex, we were unable to detect HET-C^{OR}::GFP + HET-C^{OR}::HA homocomplex in any cellular fraction (Figure 4).

HET-C heterocomplex formation is independent of het-c allele type

Strains of one *het-c* specificity (*het-c^{OR}*, *het-c^{PA}* or *het-c^{GR}*) are incompatible with strains carrying either of the other two *het-c* specificities (Howlett *et al*., 1993; Saupe and Glass, 1997; Wu and Glass, 2001). To address the question whether HET-C heterocomplex formation also occurs in other *het-c* allelic combinations [(*het-c^{GR}* + *het-c^{OR}*) and (*het-c^{GR}* + *het-c^{PA}*)], we constructed a tagged version of *het-c^{GR}* [*het-c^{GR}::GFP*; the predicted molecular weight (MW) of PM localized polypeptide is 99 kDa] (Figure 2). The *het-c^{GR}::GFP* allele was co-transformed into CJ44 with *het-c^{PA}::HA* or *het-c^{OR}::HA* alleles and the resulting incompatible transformants were assessed for HET-C heterocomplex formation by cell fractionation and co-immunoprecipitation assays. A HET-C heterocomplex was detected in the plasma membrane fraction of CJ44 (*het-c^{PA}::HA* + *het-c^{GR}::GFP*) incompatible transformants (Figure 4C). Similarly, a HET-C heterocomplex was identified in the plasma membrane fraction of CJ44

(*het-c^{OR}::HA + het-c^{GR}::GFP*) incompatible transformants (Figure 4C). Reciprocal co-immunoprecipitations gave an identical result (our unpublished data). These data showed that all allelic combinations of *het-c* that cause vegetative incompatibility are capable of forming a plasma membrane-associated HET-C heterocomplex.

The HET-C heterocomplex is associated with the plasma membrane in hyphae

To assess the organization of the HET-C heterocomplex in hyphae, we performed immunolocalization of epitope-tagged HET-C using anti-GFP and/or anti-HA antibodies and laser scanning confocal microscopy (LSCM). Using anti-GFP antibodies and Cy5-conjugated streptavidin (Cy5), HET-C^{OR}::GFP localized to the plasma membrane region in CJ44 (*het-c^{OR}::GFP + het-c^{PA}::HA*) incompatible transformants (Figure 5A and B). Similarly, using anti-HA antibodies and Alexa Fluor 488 donkey anti-rabbit IgG (Alexa 488), HET-C^{PA}::HA localized to the plasma membrane region in these same transformants (Figure 5C and D). HET-C showed an uneven distribution in hyphae of CJ44 (*het-c^{OR}::GFP + het-c^{PA}::HA*) incompatible transformants; only 20% of hyphal compartments have HET-C associated with their plasma membrane region. CJ44 transformants containing either *het-c^{OR}::GFP* and treated with anti-GFP (Cy5) (Figure 5G and H) or *het-c^{PA}::HA* and treated with anti-HA antibodies (Alexa 488; data not shown) showed only background fluorescence, consistent with the difficulty in detecting HET-C in compatible transformants by immunoprecipitation and western blot analysis (see above).

Figure 6C shows the co-localization (in yellow) of HET-C^{OR}::GFP (Figure 6A) and HET-C^{PA}::HA (Figure 6B) in a CJ44 (*het-c^{OR}::GFP + het-c^{PA}::HA*) incompatible transformant using anti-GFP (Alexa 633) and anti-HA (Alexa 488) antibodies; co-localization of HET-C^{OR}::GFP and HET-C^{PA}::HA is apparent. For better resolution, we employed deconvolution microscopy at a higher magnification. Figure 6D and E shows individual green (Alexa 488) and red (Alexa 633) signals, indicative of HET-C^{PA}::HA and HET-C^{OR}::GFP, respectively, in the plasma membrane region. Figure 6F shows a superimposed image of (D) and (E); co-localization in the plasma membrane region is indicated in yellow. Although the majority of HET-C^{OR}::GFP and HET-C^{PA}::HA co-localized, separate green (Alexa 488) and red (Alexa 633) signals were observed, suggesting that the stoichiometry between HET-C^{PA}::HA and HET-C^{OR}::GFP in these complexes may not be 1:1.

The distribution of HET-C heterocomplexes in the plasma membrane region by immunolocalization and LSCM is similar to that observed when vital dyes, such as Evans Blue, are used to stain incompatible hyphae (Jacobson *et al*., 1998; Wu and Glass, 2001): ~20% of the hyphal compartments are dead. To determine whether HCD was correlated with HET-C heterocomplex formation, we took advantage of the fact that Evans Blue emits light at 611 nm and can be visualized using a rhodamine filter set. We stained hyphae of CJ44 (*het-c^{OR}::GFP + het-c^{PA}::HA*) incompatible transformants with Evans Blue prior to the process of fixation and then treated the samples with anti-HA antibodies (Alexa 488) to detect HET-C^{PA}::HA. Figure 7A shows an image of Evans Blue fluorescence (red), while Figure 7B show plasma membrane labeling when the same sample was treated with anti-HA antibodies (Alexa 488; HET-C^{PA}::HA). (HET-C^{OR}::GFP labeling could not be assessed because of overlap in fluorescence between Evans Blue and Cy5 or Alexa 633.) Figure 7C shows a merged image of Evans Blue fluorescence and anti-HA antibody (Alexa 488) labeling (see Supplementary data). The dead hyphal compartment (marked by a white arrow) was surrounded by plasma membrane labeling associated with HET-C^{PA}::HA (Alexa 488; green).

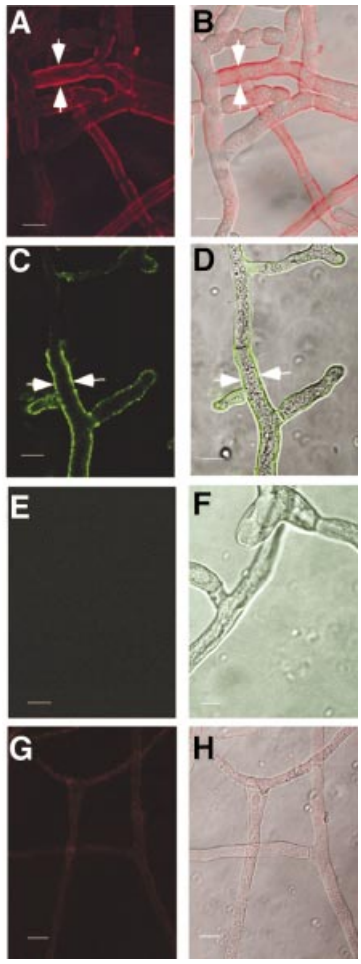

Fig. 5. HET-C heterocomplexes localize to the plasma membrane region by immunolocalization and LSCM. (**A**) A CJ44 (*het-c^{OR}::GFP + het-c^{PA}::HA*) incompatible transformant labeled with anti-GFP antibodies (Cy5). (**B**) Image in (A) superimposed onto DIC. White arrows show plasma membrane labeling. (**C**) The same transformant labeled with anti-HA antibodies (Alexa 488). (**D**) Image in (C) superimposed onto DIC. White arrows show plasma membrane labeling. (**E**) A CJ44 (*het-c^{OR} + het-c^{PA}*) untagged incompatible transformant treated with anti-HA antibodies (Alexa 488). (**F**) Image in (E) superimposed onto DIC. (**G**) A CJ44 (*het-c^{OR}::GFP*) compatible transformant treated with anti-GFP antibodies (Cy5). (**H**) The image shown in (G) superimposed onto DIC. (E–H) show a representative field; plasma membrane labeling was not observed across the entire colony. Scale bars = 10 μm.

Proper targeting of only one HET-C polypeptide is sufficient for vegetative incompatibility

Targeting to the secretory system and the plasma membrane is accomplished by a signal peptide that promotes endoplasmic reticulum (ER)-associated translation. We

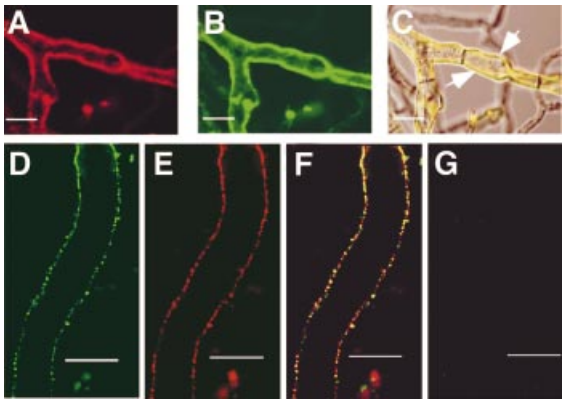

Fig. 6. HET-C^{OR}::GFP and HET-C^{PA}::HA co-localize to the plasma membrane region. (**A**) Hyphae from a CJ44 (*het-c^{OR}::GFP* + *het-c^{PA}::HA*) incompatible transformant treated with anti-GFP (Alexa 633) and (**B**) anti-HA (Alexa 488) antibodies. (**C**) An image superimposed onto DIC showing co-localization of HET-C^{OR}::GFP and HET-C^{PA}::HA in yellow (white arrows). (**D**) A deconvoluted image of a hypha from a CJ44 (*het-c^{OR}::GFP* + *het-c^{PA}::HA*) incompatible transformant in the green channel (Alexa 488; HET-C^{PA}::HA). (**E**) The same hypha in the red channel (Cy5; HET-C^{OR}::GFP). (**F**) Co-localization of anti-HA (Alexa 488; HET-C^{PA}::HA) and anti-GFP (Alexa 633; HET-C^{OR}::GFP) antibody labeling (yellow). (**G**) An untagged CJ44 (*het-c^{OR}* + *het-c^{PA}*) incompatible transformant treated with anti-GFP (Alexa 633) and anti-HA (Alexa 488) antibodies and viewed in green and red channels. Scale bars = 10 μm.

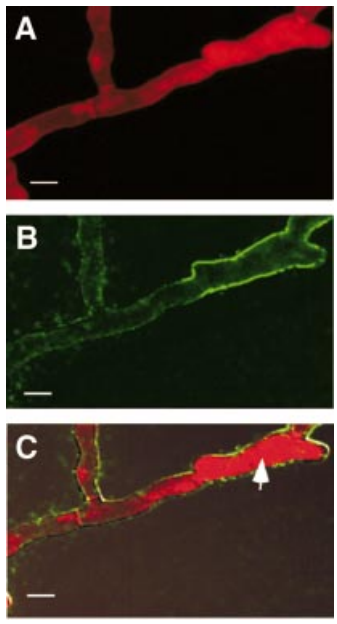

Fig. 7. HET-C heterocomplexes co-localize with dead hyphal compartments. (**A**) A CJ44 (*het-c^{OR}::GFP* + *het-c^{PA}::HA*) incompatible transformant was stained with Evans Blue and viewed with a rhodamine filter set (dead hyphal compartments show dark red). (**B**) An image of the same hyphae subsequently treated with anti-HA (Alexa 488) antibodies. (**C**) A merged image from (A) and (B). The white arrow indicates a dead cell. Scale bars = 10 μm.

therefore engineered *het-c^{OR}::GFP* and *het-c^{PA}::HA* constructs lacking signal peptides to determine whether localization to the plasma membrane was required for HET-C heterocomplex formation and vegetative incompatibility. The signal peptide deletion HET-C polypeptides are of nearly identical MW to HET-C^{OR}::GFP and HET-C^{PA}::HA; the signal peptide is removed during ER-mediated translation. Surprisingly, the Δ*sp het-c^{OR}::GFP* and Δ*sp het-c^{PA}::HA* constructs triggered vegetative incompatibility in a manner that was indistinguishable from *het-c^{OR}::GFP* and *het-c^{PA}::HA* constructs when introduced into *het-c* tester strains C2-2-1 (*het-c^{OR}*) and C9-2 (*het-c^{PA}*) (Figure 2). Figure 8A and B shows the growth rate and percentage of HCD in CJ44 (Δ*sp het-c^{PA}::HA* + *het-c^{OR}::GFP*) transformants; the morphological phenotype, growth inhibition and HCD rates (17–19%) were indistinguishable from CJ44 (*het-c^{PA}::HA* + *het-c^{OR}::GFP*) incompatible transformants.

We localized HET-C^{PA}::HA and HET-C^{OR}::GFP in CJ44 (*spΔ het-c^{OR}::GFP* + *het-c^{PA}::HA*) transformants by co-immunoprecipitation experiments. Immunoprecipitation with anti-HA antibodies and subsequent immunoblot analyses with anti-GFP antibodies revealed ~100 kDa HET-C^{OR}::GFP in the plasma membrane fraction (Figure 9A). Upon re-probing with anti-HA antibodies, an ~100 kDa HET-C^{PA}::HA protein was also detected in the plasma membrane fraction (Figure 9B). As with wild-type *het-c* constructs, HET-C^{PA}::HA or HET-C^{OR}::GFP was not detected in cellular fractions from CJ44 (Δ*sp het-c^{PA}::HA*) or CJ44 (Δ*sp het-c^{OR}::GFP*) compatible transformants, respectively (Figure 9A and B).

We performed LSCM on CJ44 (Δ*sp het-c^{PA}::HA* + *het-c^{OR}::GFP*) incompatible transformants to assess HET-C heterocomplex localization within hyphae using anti-HA antibodies. HET-C^{PA}::HA labeling (Alexa 488; green) was exclusively to the plasma membrane (Figure 9C and D; white arrows). In contrast, HET-C^{PA}::HA was not detectable in CJ44 Δ*sp het-c^{PA}::HA* compatible transformants (data not shown). These data indicate that removal of the signal peptide from one of the alternative *het-c* alleles did not affect its localization to the plasma membrane, nor its ability to trigger vegetative incompatibility.

Mis-localization of alternative HET-C polypeptides results in cytoplasmic heterocomplexes

To determine whether mis-localization of HET-C occurs when both *het-c^{PA}* and *het-c^{OR}* are missing their signal peptides, we co-transformed Δ*sp het-c^{OR}::GFP* + Δ*sp het-c^{PA}::HA* into CJ44 and characterized the resulting transformants. The CJ44 (Δ*sp het-c^{OR}::GFP* + Δ*sp het-c^{PA}::HA*) transformants did not show typical *het-c*-mediated vegetative incompatibility. As shown in Figure 8A, the CJ44 (Δ*sp het-c^{OR}::GFP* + Δ*sp het-c^{PA}::HA*) transformants initially displayed an intermediate growth rate as compared with compatible and incompatible transformants, had growth characteristics that were more similar to wild type, and formed aerial hyphae and conidia. However, cessation of growth occurred between 108 and 132 h (4.5–5.5 days) in these transformants, with growth rates falling to <0.5 cm over a 24 h period. Figure 8B shows the relationship between HCD and growth rate cessation. Between 60 and 108 h post-transformation, the percentage of HCD was 5% in the CJ44 (Δ*sp het-c^{OR}::GFP* + Δ*sp het-c^{PA}::HA*) transformants, which increased to 10% at day 5. Phenotypic differences between CJ44 transformants carrying Δ*sp het-c^{OR}::GFP* + Δ*sp het-c^{PA}::HA* constructs driven either

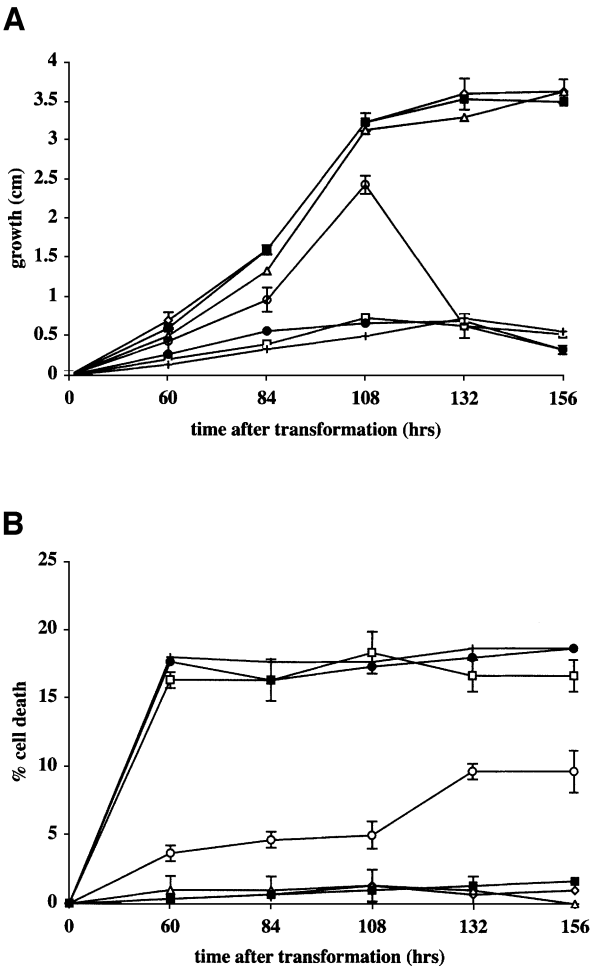

Fig. 8. Transformants containing alternative *het-c* alleles deleted for their signal peptide sequence show a novel phenotype. (**A**) Growth (in cm) was measured at 24 h intervals following transformation of CJ44 with different *het-c* constructs. Compatible transformants are CJ44 (*het-c*^{OR}) (triangles), CJ44 (*het-c*^{PA}*::HA*) (diamonds) and CJ44 (Δ*sp het-c*^{PA}*::HA*) (filled squares). Incompatible transformants are CJ44 (*het-c*^{PA} + *het-c*^{OR}) (open squares), CJ44 (*het-c*^{OR}*::GFP* + *het-c*^{PA}*::HA*) (crosses) and CJ44 (*het-c*^{OR}*::GFP* + Δ*sp het-c*^{PA}*::HA*) (filled circles). The CJ44 (Δ*sp het-c*^{OR}*::GFP* + Δ*sp het-c*^{PA}*::HA*) (open circles) transformants showed a novel phenotype. Standard deviations are shown for transformants containing compatible, incompatible and double signal peptide *het-c* deleted constructs from three separate transformants. (**B**) Percentage of HCD in transformants shown in (A), which was calculated by counting an average of 100 hyphal compartments from three independent transformants after staining with Evans Blue (Gaff and Okong'O-Ogola, 1971).

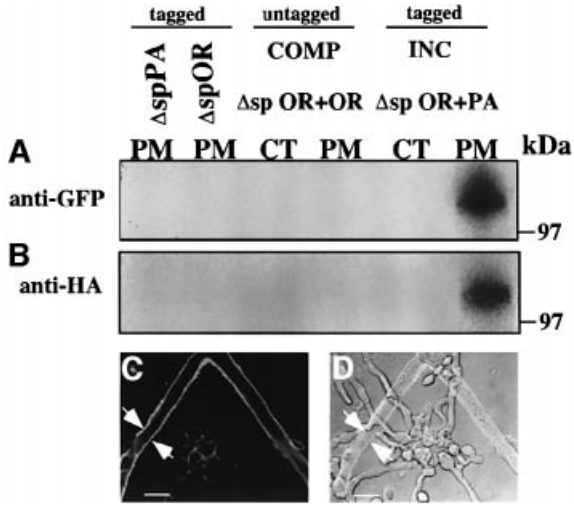

Fig. 9. Transformants containing one Δsignal peptide *het-c* construct and a wild-type alternative *het-c* allele form a HET-C heterocomplex in the plasma membrane. (**A**) Cell-fractionated samples from CJ44 (Δ*sp het-c*^{OR}*::GFP* + *het-c*^{PA}*::HA*) incompatible transformants, compatible transformants, CJ44 (Δ*sp het-c*^{OR}*::GFP* + *het-c*^{OR}*::HA*), CJ44 (Δ*sp het-c*^{OR}*::*GFP) and CJ44 (Δ*sp het-c*^{PA}*::HA*) that were subjected to immunoprecipitation by anti-HA antibodies and western analysis using anti-GFP antibodies. (**B**) The same blot stripped and re-probed with anti-HA antibodies. CT, cytoplasmic fraction; PM, plasma membrane fraction. MW markers are indicated. (**C**) A confocal image of a CJ44 (Δ*sp het-c*^{PA}*::HA* + *het-c*^{OR}*::GFP*) incompatible transformant treated with anti-HA antibodies (Alexa 488). (**D**) Image of (C) superimposed onto DIC. White arrows show plasma membrane labeling. Scale bars = 10 μm.

by the *gpd* promoter or the *het-c* promoter were not observed, consistent with results obtained with *het-c* constructs (Wu and Glass, 2001).

To determine whether HET-C heterocomplexes formed in CJ44 (Δ*sp het-c*^{OR}*::GFP* + Δ*sp het-c*^{PA}*::HA*) transformants, we performed cell fractionation and co-immunoprecipitation experiments. HET-C^{PA}::HA + HET-C^{OR}::GFP heterocomplexes were observed primarily in the cytoplasmic fraction (Figure 10A and B; CT), with a small fraction observed in the plasma membrane (Figure 10A and B; PM; Supplementary data). Both higher MW (~190 kDa) and lower MW (~90 kDa) bands were observed in both the cytoplasmic and plasma membrane fractions.

Confocal images of CJ44 (Δ*sp het-c*^{OR}*::GFP* + Δ*sp het-c*^{PA}*::HA*) transformants using anti-GFP antibodies (Alexa 633) showed cytoplasmic HET-C heterocomplexes (Figure 10C and D) as well as discrete cytoplasmic aggregates (white arrows). A similar pattern of labeling was observed when hyphae were treated with anti-HA antibodies (Alexa 488) (see Supplementary data). At a higher magnification, a deconvoluted image of a single hypha showed cytoplasmic aggregates (Figure 10E). Co-localization of anti-HA (Alexa 488) and anti-GFP (Alexa 633) antibody labeling is denoted in yellow (Figure 10F). Many aggregates do not show co-localization, suggesting that the stoichiometry between HET-C^{PA}::HA and HET-C^{OR}::GFP in these complexes may not always be 1:1.

Are cytoplasmic HET-C heterocomplexes associated with HCD in the CJ44 (Δ*sp het-c*^{OR}*::GFP* + Δ*sp het-c*^{PA}*::HA*) transformants? Figure 11 shows fluorescent images of hyphae from a CJ44 (Δ*sp het-c*^{PA}*::HA* + Δ*sp het-c*^{OR}*::GFP*) transformant stained with Evans Blue prior to fixation and immunolocalization with anti-HA antibodies (Alexa 488). Co-localization of Evans Blue fluorescence (dead hyphal compartments are red; Figure 11B) and cytoplasmic HET-C heterocomplexes (green; Figure 11C) was observed (as shown by white arrows). However, HET-C heterocomplexes were common in the cytoplasm of hyphae not stained by Evans Blue, indicating that the formation of the cytoplasmic HET-C heterocomplexes may not always be associated with HCD (Figure 11A–C; yellow arrows).

CJ44 transformants containing signal peptide deletion constructs of identical *het-c* specificity (Δ*sp het-c*^{OR}*::GFP* + Δ*sp het-c*^{OR}*::HA*) were phenotypically similar to

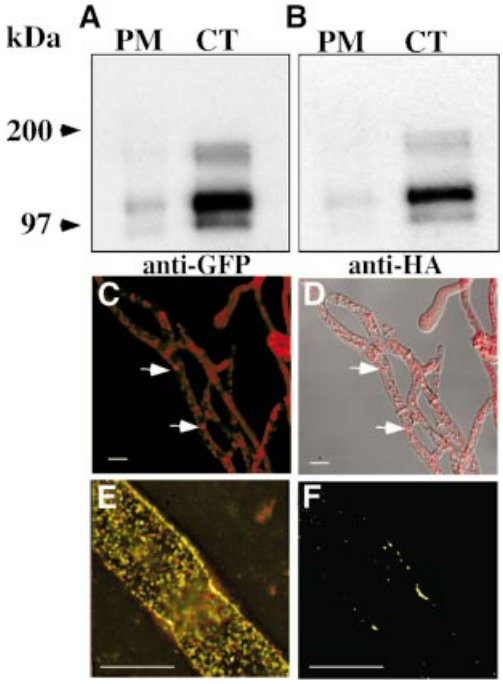

Fig. 10. HET-C heterocomplexes localize to the cytoplasm in transformants containing dual Δsignal peptide *het-c* constructs. (**A**) Cell fractions from a CJ44 (Δ*sp het-c*^{PA}*::HA* + Δ*sp het-c*^{OR}*::GFP*) transformant subjected to immunoprecipitation with anti-HA antibodies and western analysis using anti-GFP antibodies. (**B**) The same immunoblot after stripping and re-probing with anti-HA antibodies. PM, plasma membrane fraction; CT, cytoplasmic fraction. MW markers are indicated. (**C**) A confocal image of hyphae from a CJ44 (Δ*sp het-c*^{PA}*::HA* + Δ*sp het-c*^{OR}*::GFP*) transformant treated with anti-GFP (Alexa 633) antibodies. White arrows show cytoplasmic aggregates. (**D**) Image in (C) merged with DIC. (**E**) A deconvoluted image of a single hypha from a CJ44 (Δ*sp het-c*^{PA}*::HA* + Δ*sp het-c*^{OR}*::GFP*) transformant treated with both anti-HA (Alexa 488; green) and anti-GFP (Alexa 633; red) antibodies viewed with red and green channels. (**F**) Co-localization (yellow) of only HET-C^{OR}::GFP and HET-C^{PA}::HA using the Bitplane co-localization program on the image in (E). Scale bars = 10 μm.

wild-type compatible transformants. We were unable to detect a ~100 kDa HET-C^{OR}::HA or HET-C^{OR}::GFP polypeptide in any cellular fraction of CJ44 (Δ*sp het-c*^{OR}*::GFP* + Δ*sp het-c*^{OR}*::HA*) compatible transformants by co-immunoprecipitation, immunoprecipitation and western blot analyses (data not shown).

Discussion

The results of this study demonstrate that physical interaction of HET-C polypeptides encoded by *het-c* alleles of alternative specificity mediates nonself recognition during vegetative incompatibility in *N.crassa* and is a significant step in our understanding of how vegetative incompatibility is triggered. The presence of HET-C heterocomplexes in the plasma membrane is associated with the phenotypic aspects of vegetative incompatibility, namely, growth inhibition, repression of conidiation and HCD (Garnjobst and Wilson, 1956; Perkins, 1975; Jacobson *et al*., 1998). Nonself recognition mediated by HET-C heterocomplex formation was not restricted to one *het-c* allelic pair, but occurred in all combinations of *het-c* alleles that mediate vegetative incompatibility. In *Podospora anserina,* it has been shown using yeast two-hybrid experiments that both homo- and heterocomplexes are formed by proteins encoded by alternative specificities at the vegetative incompatibility locus, *het-s* (Coustou *et al*., 1997). Presumably, nonself recognition leading to vegetative incompatibility is also mediated by HET-S–HET-s heterocomplex formation. These observations suggest that heterocomplex formation between alternative HET proteins may be a common theme in nonself recognition during vegetative incompatibility.

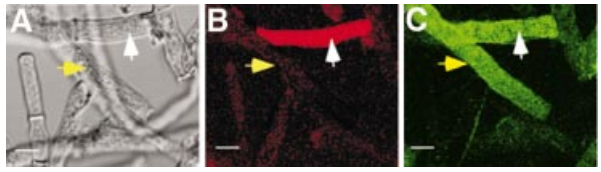

Fig. 11. Cytoplasmic HET-C heterocomplexes do not always co-localize with dead hyphal compartments. (**A**) A DIC image of hyphae from a CJ44 (Δ*sp het-c*^{PA}*::HA* + Δ*sp het-c*^{OR}*::GFP*) incompatible transformant. (**B**) Transformant in (A) after staining with Evans Blue (rhodamine filter set). (**C**) The same field of hyphae showing labeling by anti-HA antibodies (HET-C^{PA}::HA; Alexa 488). The white arrow in (A), (B) and (C) shows a dead hyphal compartment. The yellow arrow in (A), (B) and (C) shows a live hyphal compartment. Scale bars = 10 μm.

HET-C heterocomplexes were abundant and readily detectable in the plasma membrane of incompatible transformants both by co-immunoprecipitation assays and by immunofluorescence using LSCM. However, under identical conditions, HET-C by itself or as a HET-C homocomplex was undetectable. We enriched for HET-C by using aminolink chromatography and cellular fractionation; HET-C was identified in the plasma membrane fraction. Similar differences in affinity between homo- and heterocomplexes have been described for Fos–Jun protein interactions in mammalian systems. Heterodimer formation is largely a thermodynamic consequence of Fos homodimer instability: Fos and Jun preferentially form a heterodimer (O'Shea *et al*., 1992). In *U.maydis,* heterodimer formation between homeodomain proteins encoded by different *b* alleles mediates nonself recognition (Kämper *et al*., 1995). Protein complexes between homeodomain proteins from the same *b* allele were not detectable. It is possible that the formation of a HET-C heterocomplex induces a conformational change in HET-C or causes the recruitment of other proteins to the HET-C heterocomplex that 'mask' protease degradation sites, thus rendering HET-C heterocomplexes more stable. Alternatively, regulation of HET-C protein stability may be determined by the activity of another protein, such as has been observed between the p53 tumor-suppressor protein and Mdm2: Mdm2 promotes the rapid degradation of p53 (Haupt *et al*., 1997).

According to topology predictions, the *het-c* specificity domain resides in the cytoplasm. The lack of the signal peptide in one of the HET-C polypeptides results in the formation of a HET-C heterocomplex that still localizes to the plasma membrane and is sufficient to cause a classical *het-c* vegetative incompatible phenotype. However, the signal peptide of *het-c* is essential for proper targeting because transformants containing alternative *het-c* alleles that are both deleted for their signal peptide resulted in primarily cytoplasmic localization of HET-C heterocomplexes.

Is the localization of HET-C heterocomplexes to the plasma membrane a prerequisite for vegetative incompatibility? Several lines of evidence suggest that it is. HET-C heterocomplexes are associated with the plasma membrane region of dead hyphal compartments. The mislocalization of alternative HET-C polypeptides resulted in the formation of HET-C heterocomplexes in the cytoplasm of both dead and live hyphal compartments. Transformants containing cytoplasmic HET-C heterocomplexes initially grew at a rate near that of compatible transformants and formed aerial hyphae and conidia, but underwent growth arrest at ~5 days of growth. Thus, localization of HET-C to the plasma membrane is required for typical phenotypic aspects of vegetative incompatibility, including repression of conidiation, HCD and growth inhibition. The formation of HET-C heterocomplexes, as well as their cellular localization is, we believe, one of the key factors in triggering vegetative incompatibility.

What is the nature of the HET-C heterocomplex? Deconvolution data of HET-C heterocomplexes in the plasma membrane and cytoplasm showed co-localization of HET-C^{PA}::HA and HET-C^{OR}::GFP, but also complexes that appeared to be primarily HET-C^{PA}::HA or HET-C^{OR}::GFP. Large aggregates were observed in the cytoplasm of transformants bearing *het-c* constructs deleted for their signal peptide sequence, suggesting that the HET-C heterocomplex can be of complex structure. The stoichiometric ratio of individual HET-C molecules in the heterocomplex is unclear. It has been shown that a *het* protein in a filamentous fungus, *P.anserina*, HET-s, forms protease-resistant aggregates (Coustou *et al*., 1997, 1999) and forms multimers even under denaturing conditions. HET-s has been show to function as a prion analog (Coustou *et al*., 1997; Wickner *et al*., 1999). In *S.cerevisiae*, oligopeptide repeats GGYGGT and SQPSYG in the N-terminal domain of Sup35p are involved in spontaneous propagation of novel [*PSI*$^+$] prion elements (Nakayashiki *et al*., 2001). HET-C has eight repeats (partial or perfect) of the SQPSYG motif and six repeats of the GGYGGY motif from amino acids 708 to 951. However, deletion analysis of *het-c* showed that only part of the glycine-rich domain (from amino acids 610 to 730) is essential for vegetative incompatibility (Saupe *et al*., 1996; G.Iyer, unpublished results).

The indel motif in the *het-c* specificity domain (Figure 1) is sufficient to confer *het-c* allelic specificity (Saupe and Glass, 1997; Wu and Glass, 2001). Structural aspects of the *het-c* specificity domain must also regulate the capacity for alternative HET-C polypeptides to form a heterocomplex. It is unclear whether physical interactions between alternative HET-C polypeptides is mediated by the *het-c* specificity domain, or whether variations in this region affect the conformation of another region (such as the glycine-rich domain) that may be involved in physical interaction of alternative HET-C polypeptides. We are currently conducting experiments to determine the topology of HET-C in the plasma membrane, the region of physical interaction between alternative HET-C polypeptides and specific amino acid requirements of both the glycine-rich repeats and the specificity domain for HET-C heterocomplex formation.

How do plasma membrane-bound HET-C heterocomplexes mediate the pleiotropic phenotype associated with vegetative incompatibility? Two hypotheses are plausible. First, it is possible that HET-C heterocomplex formation acts as a signal to activate pathways associated with conidiation repression, growth inhibition and HCD. Activation of signal transduction pathways has been associated with programmed cell death in eukaryotes (Wilson, 1998). Alternatively, it is possible that the formation of HET-C heterocomplexes in the PM compromises plasma membrane function, thus destabilizing the hyphal compartment and causing death, perhaps by induction of a stress response pathway. It has been proposed that *het* genes encode products that form 'poison' heterocomplexes that lead to a lethal disorder (Bégueret *et al*., 1994). Septal plugging, a hallmark of the hyphal compartmentation during vegetative incompatibility, can also be induced by injury (Jedd and Chua, 2000). We have begun a genetic dissection of *het-c*-mediated vegetative incompatibility to differentiate these two hypotheses and to understand how the formation of HET-C heterocomplexes in the PM leads to the dramatic consequences of vegetative incompatibility.

Materials and methods

Strains and culture conditions

Escherichia coli DH5α (Bethesda Research Laboratories) was used for bacterial transformation (Sambrook *et al*., 1989) and plasmid maintenance. *N.crassa* strains used were C9-2 (*thr-2 het-c^{PA} a*), C2-2-9 (*thr-2 het-c^{OR} A)* (Saupe *et al*., 1996) and CJ44 (*pan-2 arg-5 Δhet-c A*) (Wu and Glass, 2001). Strains were grown on Vogel's medium (VM) (Vogel, 1964) with required supplements.

het-c constructs

The *het-c^{OR}::GFP* vector was constructed as described in Wu (2000). Constructs were cloned into either pOKE103 (gift from R.Metzenberg), which confers pantothenate prototrophy, or pCB1004 (Carroll *et al*., 1994), which confers hygromycin resistance. The *het-c^{GR}::GFP* vector was constructed by 'swapping' a 588 bp *Eco*RV–*Stu*I fragment containing the specificity domain of *het-c^{GR}* into the *het-c^{OR}::GFP* vector. The *het-c^{PA}::HA* construct was made by amplifying a 3.2 kb *het-c^{PA}* product using primers from *Sca*I 5′ SS.1 (AGTACTGCGCTACTAGCTACTAGA) and a 3′ primer SS.2 (GAGCTCGAACATCGGAGGTAT**TACCCTTATGATGTGCCAGATTATGCC**TGA) with a *Sac*I site, the *het-c^{PA}* sequence from amino acids 970–974, plus 27 nucleotides of HA sequence followed by a stop codon. The *HA* sequence is in bold; restriction sites are underlined.

The 650 bp *gpd* promoter fragment (Punt *et al*., 1988) was amplified using primers SS.3 5′-GCATGCCATTAACCTAGGTA-3′ and SS.4 5′-AGATCTGTAACACTACAGACGATG-3′ as a *Sph*I–*Xba*I fragment. The *GFP* ORF was ligated as a *Sac*I–*Eco*R I fragment using primers SS.5 (GAGCTCATGGAGCAAGGGCGAGGAACT) and SS.6 (GAATTCACGAGCTGTACAAGTTGA). Primers containing sequences eliminating the signal peptide (amino acids 1–30) for *het-c^{OR}* were used to amplify a 2.4 kb *Xba*I–*Sac*I product, which was inserted into the *gpd-GFP* plasmid. Primers SS.7 (TCTAGAGCTGGCAACATTCCCTCCATC) and SS.8 (GAGCTCATCCTTCGCAGCCGTCATAT) contain *Xba*I and *Sac*I sites, respectively. For the Δ*sp het-c^{PA}::HA* construct, a primer containing a *Xba*I site, SS.9 (TCTAGAGCTGCAGCCTTCGGTGCTGGC) was used with primer SS.2 to amplify a 3.1 kb *het-c^{PA}* product. The *het-c* constructs were made by subcloning *Xba*I–*Sac*I fragments from amino acid residues 2–730 and 2–974 of *het-c^{OR}::GFP* and *het-c^{PA}::HA*. Differences in the percentage of HCD, growth inhibition rate or other phenotypic characteristics associated with *het-c* incompatibility were not observed when the *het-c* promoter was replaced with the *gpd* promoter (this study and S.Sarkar, unpublished results). All constructs were verified by DNA sequencing and their functionality verified *in vivo*.

Neurospora transformation

Neurospora strains were transformed as described previously (Wu and Glass, 2001). For co-transformation experiments using pCB1004 and

pOKE constructs, transformants were selected for both hygromycin resistance (250 μg/ml) and restoration of pantothenate prototrophy.

Microscopic analysis and cell death/growth inhibition assays

Growth of strains was measured at 24 h intervals using race tubes containing supplemented VM (Davis and De Serres, 1970). Evans Blue staining was carried out according to Jacobson *et al*. (1998). Evans Blue enters permeabilized cells and binds irreversibly to intracellular proteins (Gaff and Okong'O-Ogola, 1971). Samples were examined under bright field illumination on a Zeiss Axioskop or Zeiss LS 750 microscope for fluorescence with a rhodamine filter set. The percentage of dead hyphal compartments was determined by examining three independent compatible or incompatible transformants and calculating the number of dead cells per 100 hyphal compartments counted in a field.

Isolation and extraction of organelle fractions

Cell fractionation procedures using *Neurospora* were as described previously (Bowman and Bowman, 1988), in which separation of cellular fractions is performed by a series of centrifugation steps. To assess cell fractionation procedures, we used polyclonal antibodies to the *N.crassa* PM H^+-ATPase (dilution 1:5000 as recommended; gift from the C.Slayman laboratory) (Bowman *et al*., 1981) and monoclonal antibody (clone TU27) against β-tubulin (dilution 1:2000; BAbCO), a cytoplasmic marker. The cell wall fraction is from a pellet following disruption of mycelia and centrifugation at 1000 *g*, which was subsequently resuspended in 50 mM HEPES pH 7.5, 10 mM NaCl, 0.1% NP-40, 0.05% sodium deoxycholate and homogenized. The resulting supernatant was concentrated prior to use, similar to other cellular fractions.

Protein extraction and affinity purification

An anti-HA aminolink column was prepared according to the manufacturer's specifications (Pierce). Proteins from cytoplasmic (2.4 mg/ml), PM (0.5 mg/ml) and cell wall (1.1 mg/ml) fractions were loaded onto the anti-HA aminolink column, incubated and washed with seven columns of binding buffer. Eluates were subjected to immunoblotting with anti-HA antibodies. Immunodetection was carried out according to the manufacturer's specifications (ECL kit; Amersham).

Co-immunoprecipitation experiments

Approximately 0.5 mg of protein extract from various cellular fractions were incubated at 4°C for 6 h with either anti-GFP (1:1500 dilution; Roche Biochemicals) or monoclonal anti-HA antibodies (clone 12CA5; 1:1000 dilution; Roche). Protein G–agarose beads (50 μl; Roche) were added; immunoprecipitation was according to the manufacturer's specifications. Washing was repeated twice with a modified lysis buffer (50 mM HEPES pH 7.5, 750 mM NaCl, 0.1% NP-40, 0.05% sodium deoxycholate) with a final wash in the above buffer, but omitting NaCl. The resulting pellet was subjected to electrophoresis on an 8% SDS–PAGE gel and analyzed by immunoblotting, as above.

LSCM and immunofluorescence

Antibodies for LSCM were mouse anti-GFP mAb (Roche), biotinylated goat anti-mouse IgG (H+L) (Roche), Cy5-conjugated streptavidin (Jackson ImmunoResearch), goat anti-HA rabbit polyclonal antibody (Santa Cruz Biotechnologies), Alexa Fluor 488-conjugated donkey anti-rabbit IgG and Alexa Fluor 633-conjugated goat anti-mouse IgG (Molecular Probes).

Neurospora crassa hyphae were prepared for confocal microscopy as described in Tinsley *et al*. (1998), which involved cryofixation of hyphal tissue by plunging into liquid propane (purchased commercially). Incubation was for 4 h for the primary antibody (200 μg/ml) and for 2 h for the secondary antibody (5 μg/ml). During single-labeling experiments, the extent of red/green 'bleed through' was checked in the appropriate channels. Staining for co-localization of HET-C^{OR}::GFP and HET-C^{PA}::HA was performed as follows: hyphae were incubated with both anti-GFP and anti-HA primary antibodies, followed by washing and incubation with the appropriate secondary antibodies, washed and mounted. Microscopes used were Zeiss LSM 510 for confocal with DIC optics (Plan-Apo 63×/1.25 N.A. objective) and API wide-field deconvolution microscope (Plan-Neo 100×/1.3 N.A. objective). Data were analyzed using Deltavision software (version 2.5) and the Imaris Bitplane co-localization (version 3.0) program. Alexa Fluor 488 was detected by excitation at 488 nm, emission at 505/550 nm. Cy5 and Alexa Fluor 633 were detected by excitation at 633 nm, emission long pass 650 nm.

Supplementary data

Supplementary data are available at *The EMBO Journal* Online.

Acknowledgements

We wish to thank Drs Steve Ruzin, Denise Schichnes (CNR Imaging Facility) and Kent Macdonald (Electron Microscopy Unit) for valuable assistance and technical support for microscopy. We acknowledge the help of Drs Sven Saupe and Richard Todd in making some of the *het-c* constructs. We are grateful to the C.Slayman laboratory for the gift of H^+-ATPase antibodies. We thank Drs Sven Saupe and Bob Metzenberg for their critical reading of the manuscript. The work reported in this paper was supported by a grant from the National Institutes of Health (GM60468-01) to N.L.G.

References

Asante-Owusu,R.N., Banham,A.H., Böhnert,H.U., Mellor,E.J. and Casselton,L.A. (1996) Heterodimerization between two classes of homeodomain proteins in the mushroom *Coprinus cinereus* brings together potential DNA-binding and activation domains. *Gene*, **172**, 25–31.

Bégueret,J., Turcq,B. and Clave,C. (1994) Vegetative incompatibility in filamentous fungi—*het* genes begin to talk. *Trends Genet.*, **10**, 441–446.

Bowman,B.J., Blasco,F. and Slayman,C.W. (1981) Purification and characterization of the plasma membrane ATPase of *Neurospora crassa*. *J. Biol. Chem.*, **256**, 12343–12349.

Bowman,E.J. and Bowman,B.J. (1988) Purification of vacuolar membranes, mitochondria and plasma membranes from *Neurospora crassa* and modes of discriminating among the different H^+-ATPases. *Methods Enzymol.*, **157**, 562–573.

Carroll,A.M., Sweigard,J.A. and Valent,B. (1994) Improved vectors for selecting resistance to hygromycin. *Fungal Genet. Newsl.*, **41**, 22.

Cormack,B. (1998) Green fluorescent protein as a reporter of transcription and protein localization in fungi. *Curr. Opin. Microbiol.*, **1**, 406–410.

Cortesi,P., McCulloch,C.E., Song,H., Lin,H. and Milgroom,M.G. (2001) Genetic control of horizontal virus transmission in the chestnut blight fungus, *Cryphonectria parasitica*. *Genetics*, **159**, 107–118.

Coustou,V., Deleu,C., Saupe,S. and Bégueret,J. (1997) The protein product of the *het-s* heterokaryon incompatibility gene of the fungus *Podospora anserina* behaves as a prion analog. *Proc. Natl Acad. Sci. USA*, **94**, 9773–9778.

Coustou,V., Deleu,C., Saupe,S.J. and Bégueret,J. (1999) Mutational analysis of the [Het-s] prion analog of *Podospora anserina*. A short N-terminal peptide allows prion propagation. *Genetics*, **153**, 1629–1640.

Davis,R.H. and De Serres,F.J. (1970) Genetic and microbial research techniques for *Neurospora crassa*. *Methods Enzymol.*, **17A**, 79–143.

Debets,A.J.M. and Griffiths,A.J.F. (1998) Polymorphism of *het*-genes prevents resource plundering in *Neurospora crassa*. *Mycol. Res.*, **102**, 1343–1349.

Forsburg,S.L. and Sherman,D.A. (1997) General purpose tagging vectors for fission yeast. *Gene*, **191**, 191–195.

Gaff,D.F. and Okong'O-Ogola,O. (1971) The use of non-permeating pigments for testing the survival of cells. *J. Exp. Bot.*, **22**, 756–758.

Garnjobst,L. and Wilson,J.F. (1956) Heterocaryosis and protoplasmic incompatibility in *Neurospora crassa*. *Proc. Natl Acad. Sci. USA*, **42**, 613–618.

Glass,N.L., Jacobson,D.J. and Shiu,K.T. (2000) The genetics of hyphal fusion and vegetative incompatibility in filamentous ascomycetes. *Annu. Rev. Genet.*, **34**, 165–186.

Haupt,Y., Maya,R., Kazaz,A. and Oren,M. (1997) Mdm2 promotes the rapid degradation of p53. *Nature*, **387**, 296–299.

Ho,C., Adamson,J.G., Hodges,R.S. and Smith,M. (1994) Heterodimerization of the yeast MAT**a1** and Mat**a2** proteins is mediated by two leucine zipper-like coiled-coil motifs. *EMBO J.*, **13**, 1403–1413.

Howlett,B., Leslie,J.F. and Perkins,D.D. (1993) Putative multiple alleles a the vegetative (heterokaryon) incompatibility loci *het-c* and *het-8* in *Neurospora crassa*. *Fungal Genet. Newsl.*, **40**, 40–42.

Jacobson,D.J., Beurkens,K. and Klomparens,K.L. (1998) Microscopic and ultrastructural examination of vegetative incompatibility in partial

diploids heterozygous at *het* loci in *Neurospora crassa*. *Fungal Genet. Biol.*, **23**, 45–56.
Jedd,G. and Chua,N.H. (2000) A new self-assembled peroxisomal vesicle required for efficient resealing of the plasma membrane. *Nat. Cell Biol.*, **2**, 226–231.
Jones,E.Y., Tormo,J., Reid,S.W. and Stuart,D.I. (1998) Recognition surfaces of MHC class I. *Immunol. Rev.*, **163**, 121–128.
Kämper,J., Reichmann,M., Romeis,T., Bölker,M. and Kahmann,R. (1995) Multiallelic recognition: nonself-dependent dimerization of the bE and bW homeodomain proteins in *Ustilago maydis*. *Cell*, **81**, 73–83.
Klein,J., Sato,A., Nagl,S. and O'hUigin,C. (1998) Molecular trans-species polymorphism. *Annu. Rev. Ecol. Syst.*, **29**, 1–21.
May,G., Shaw,F., Badrane,H. and Vekemans,X. (1999) The signature of balancing selection: fungal mating compatibility gene evolution. *Proc. Natl Acad. Sci. USA*, **96**, 9172–9177.
Nakayashiki,T., Ebihara,K., Bannai,H. and Nakamura,Y. (2001) Yeast [PSI+] 'prions' that are crosstransmissible and susceptible beyond a species barrier through a quasi-prion state. *Mol. Cell*, **7**, 1121–1130.
Nasrallah,J.B. (2000) Cell–cell signaling in the self-incompatibility response. *Curr. Opin. Plant Biol.*, **3**, 368–373.
O'Shea,E.K., Rutkowski,R. and Kim,P.S. (1992) Mechanism of specificity in the Fos–Jun oncoprotein heterodimer. *Cell*, **68**, 699–708.
Perkins,D.D. (1975) The use of duplication-generating rearrangements for studying heterokaryon incompatibility genes in *Neurospora*. *Genetics*, **80**, 87–105.
Perkins,D.D., Radford,A. and Sachs,M.S. (2000) *The Neurospora Compendium: Chromosomal Loci.* Academic Press, San Diego, CA.
Pontecorvo,G. (1956) The parasexual cycle in fungi. *Annu. Rev. Microbiol.*, **10**, 393–400.
Punt,P.J., Dingemanse,M.A., Jacobs-Meijsing,B.J., Pouwels,P.H. and van den Hondel,C.A. (1988) Isolation and characterization of the glyceraldehyde-3-phosphate dehydrogenase gene of *Aspergillus nidulans*. *Gene*, **69**, 49–57.
Sambrook,J., Fritsch,E.F. and Maniatis,T. (1989) *Molecular Cloning: A Laboratory Manual*. Cold Spring Harbor Laboratory Press, Cold Spring Harbor, NY.
Saupe,S.J. (2000) Molecular genetics of heterokaryon incompatibility in filamentous ascomycetes. *Microbiol. Mol. Biol. Rev.*, **64**, 489–502.
Saupe,S.J. and Glass,N.L. (1997) Allelic specificity at the *het-c* heterokaryon incompatibility locus of *Neurospora crassa* is determined by a highly variable domain. *Genetics*, **146**, 1299–1309.
Saupe,S.J., Kuldau,G.A., Smith,M.L. and Glass,N.L. (1996) The product of the *het-c* heterokaryon incompatibility gene of *Neurospora crassa* has characteristics of a glycine-rich cell wall protein. *Genetics*, **143**, 1589–1600.
Tinsley,J.H., Lee,I.H., Minke,P.F. and Plamann,M. (1998) Analysis of actin and actin-related protein 3 (ARP3) gene expression following induction of hyphal tip formation and apolar growth in *Neurospora*. *Mol. Gen. Genet.*, **259**, 601–609.
Vogel,H.J. (1964) Distribution of lysine pathways among fungi: evolutionary implications. *Am. Nat.*, **98**, 435–446.
Wickner,R.B. Taylor,K.L., Edskes,H.K., Maddelein,M.L., Moriyama,H. and Roberts,B.T. (1999) Prions in *Saccharomyces* and *Podospora* spp.: protein-based inheritance. *Microbiol. Mol. Biol. Rev.*, **63**, 844–861.
Wilson,M.R. (1998) Apoptotic signal transduction: emerging pathways. *Biochem. Cell Biol.*, **76**, 573–582.
Wu,J. (2000) Non-self recognition in filamentous fungi—the *het-c* mediated vegetative incompatibility in *Neurospora crassa*. Ph.D. thesis, Botany Department and The Biotechnology Laboratory, University of British Columbia, Vancouver, Canada.
Wu,J. and Glass,N.L. (2001) Identification of specificity determinants and generation of alleles with novel specificity at the *het-c* heterokaryon incompatibility locus of *Neurospora crassa*. *Mol. Cell. Biol.*, **21**, 1045–1057.
Wu,J., Saupe,S.J. and Glass,N.L. (1998) Evidence for balancing selection operating at the *het-c* heterokaryon incompatibility locus in a group of filamentous fungi. *Proc. Natl Acad. Sci. USA*, **95**, 12398–12403.

Received January 10, 2002; revised July 5, 2002; accepted July 19, 2002